PCCP

PAPER

View Article Online
View Journal | View Issue

Cite this: *Phys. Chem. Chem. Phys.*, 2019, **21**, 25054

Singlet oxygen partition between the outer-, inner- and membrane-phases of photo/chemotherapeutic liposomes†

Vladimir Kabanov, [a] Sanjana Ghosh,[b] Jonathan F. Lovell [b] and Belinda Heyne *[a]

Received 19th September 2019,
Accepted 11th October 2019

DOI: 10.1039/c9cp05159g

rsc.li/pccp

Liposomes carrying membrane-embedded porphyrin-phospholipid (PoP) are capable of chemo- and photo-therapeutic modes of action, which make them a potential candidate material for next-generation cancer treatments. This study examines singlet oxygen ($^1O_2$) production and release by PoP liposomes carrying either no chemotherapeutic cargo (EMPTY), or those carrying either doxorubicin (DOX) or irinotecan (IRT) chemotherapy drugs. Herein, we developed a strategy to quantify the fraction of $^1O_2$ lifetime spent in the three distinct local liposomal environments by obtaining four key pieces of information for each system: average $^1O_2$ deactivation rate constants (k_Δ) for liposome suspensions in H_2O and in D_2O solvents, as well as the absolute and the apparent $^1O_2$ production quantum yields (Φ_Δ). Despite the characteristic differences in their photophysical behavior, namely in Φ_Δ values, all three formulations of PoP liposomes were found to carry out $^1O_2$ release in a similar manner. It was found that >80% of all sensitized $^1O_2$ from the ensemble of PoP liposomes deactivates within the nanostructures themselves, with the largest portion (~50%) deactivating in the lipid membrane specifically. Based on these findings, we conclude that the current design of the PoP liposomes is well suited for light-induced chemotherapeutic drug release. Importantly, the $^1O_2$ partition quantification approach reported herein has potential to be a tool for characterizing nanoparticulate light-activated chemo- and phototherapeutic systems.

Introduction

Over the last few decades, photodynamic therapy (PDT) has become a major topic of investigation as an alternative treatment method for cancer and infectious diseases.[1] Unlike conventional chemotherapy, PDT relies on the process of photosensitization, *i.e.* light-induced production of cytotoxic reactive oxygen species from a chromophore (photosensitizer, PS).[2,3] This mode of action inherently gives PDT an advantage of being a more spatio-temporally controlled tumour treatment strategy.[4] While PDT is gaining momentum to be applied in the clinic for the treatment of skin, oral and lung conditions,[5,6] to this day it is not widely accepted as a frontline therapy for deeper lying solid tumours.[7] One of the challenges preventing broader PDT application is the very nature of the photosensitization process, that is, its reliance on the photosensitizer's ability to absorb photons through tissues.[2,3] Even red or near infrared light penetrates tissues only to a couple of centimetres' depth. Thus, for deeper tumours, this leads to the lack of, or generally poor, PS excitation and, ultimately, the inability of the photosensitization process to produce a sufficient amount of cytotoxic species for tumour destruction under reasonable irradiation conditions.[3,8]

Recent advancements in materials science, especially nano-science, have provided possible mitigations to this problem.[7,9,10] Solutions such as two photon absorbing nanomaterials,[11] photon up-conversion nanoparticles,[12] and organic–inorganic hybrid nanomaterials,[13] to name a few, have all been proposed and studied in the literature. However, these methods rely on complex photophysical and quantum phenomena, and are not yet easily accessible.[7] On the other hand, novel materials which combine both the photo- and the chemo-therapeutic modes of action are within closer reach to see widespread clinical applications.[14,15] Such materials commonly consist of a chemo-drug encapsulated in a nanoparticle carrier equipped with a light triggered drug release mechanism.[16] This design benefits from keeping the drug dormant unless acted upon by a photo-stimulus, making it less harmful than classical chemo-therapy. Meanwhile, the photosensitization process only needs

[a] *Department of Chemistry, University of Calgary, 2500 University Drive NW, Calgary, Alberta, T2N 1N4, Canada. E-mail: bjmheyne@ucalgary.ca*
[b] *Department of Biomedical Engineering, University at Buffalo, Buffalo, NY, 14260, USA*

† Electronic supplementary information (ESI) available: Detailed synthetic procedures, instrumentation, UV-vis deconvolution, steady-state and time-resolved fluorescence emission, drug release experiments, and control experiments for the direct and the indirect detection of singlet oxygen. See DOI: 10.1039/c9cp05159g

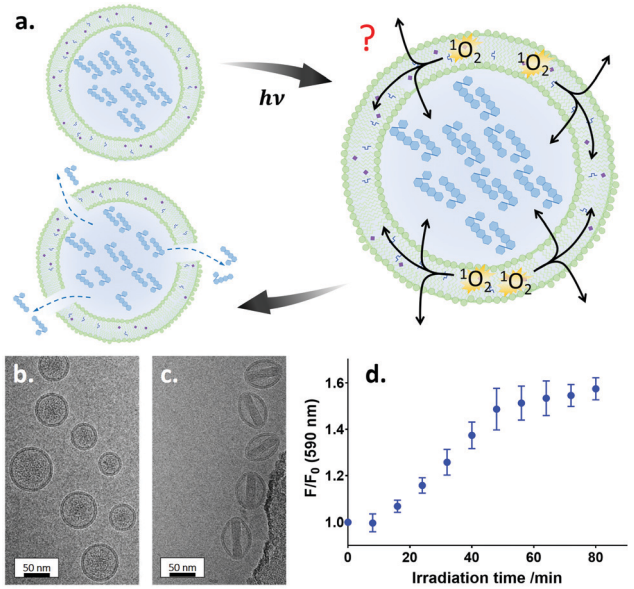

Fig. 1 (a) Cartoon representation of the drug-loaded PoP liposomes' dual modes of action. Upon irradiation singlet oxygen is produced in the lipid membrane of the liposomes and can further diffuse into the inner-, outer-, or membrane-liposomal environments (as represented by the thin arrows) before activating a drug release mechanism *via* the unsaturated lipid oxidation.[22] The question mark refers to the main focus of this study, *i.e.* determining the fraction of lifetime which $^1O_2$ spends in each local liposomal environment. (b) and (c) are previously reported[18] transmission electron microscope images of IRT@PoP and DOX@PoP liposomes, respectively (reproduced under the terms of the Creative Commons Attribution (CC BY-NC) License). (d) DOX release kinetics from DOX@PoP liposomes in H_2O, as characterized *via* steady-state fluorescence emission[23] (293 K, 110 mW from a CW halogen lamp (300 W, 80 V) mounted on a slide projector (Kodak) equipped with a 625 nm high-pass filter). Error bars represent ± standard deviation obtained from triplicate measurements.

to produce enough reactive oxygen species to locally trigger the drug release.[14]

Among a suite of dual action chemo- and photo-therapeutic materials, liposomes with membrane-bound porphyrins (porphysomes, PoP) which can encapsulate a variety of clinically approved chemotherapeutic drugs (Fig. 1a–c) have gained attention.[17–21] Our study employs three formulations of these liposomes: EMPTY PoP, doxorubicin loaded PoP (DOX@PoP), and irinotecan loaded PoP (IRT@PoP).

From previous studies, it has been suggested that excitation of the porphyrin in the PoP liposomes initiates singlet oxygen ($^1O_2$) production in the lipid membrane (Fig. 1a).[22] The produced $^1O_2$ can diffuse through the membrane which contains a combination of saturated and unsaturated fatty acids. It has been shown in multiple studies that the unsaturated lipids undergo PoP-mediated photo-oxidization, likely by reacting with $^1O_2$ and, upon reaching a threshold level of photooxidation, enough of the liposome membrane is disturbed to allow the release of the encapsulated chemo-drug (Fig. 1d).[15,22,24]

It is evident that the amount of $^1O_2$ produced *via* the photosensitization process in the PoP liposomes (*i.e.* the quantum yield of $^1O_2$ production, Φ_Δ) dictates the photodynamic efficiency of the treatment, in this case the drug release kinetics of the system.[22,25,26] However, perhaps less evidently, there is an extra layer of complexity hidden in the PoP liposome design. In order to fully describe the drug-release dependence on the photosensitization efficiency, one must also consider the amount of $^1O_2$ which is released into the bulk solution *vs.* the amount which resides in the lipid membrane specifically.[27] Furthermore, it is also important to consider and quantify the amount of $^1O_2$ diffusing into the inner liposomal cavity, which may be detrimental to the whole treatment efficiency. To date, the kinetic parameters governing the behavior of the $^1O_2$ produced from the PoP liposomes have not been reported. Although, the material has already been shown to be an efficient tumor battling agent,[17,21] we believe that understanding the partition of $^1O_2$ between the inner-, outer- and membrane-local environments of the liposomes is critical for the current and future engineering of liposome-based photodynamic systems, and their downstream clinical applications.

The overall rate of $^1O_2$ deactivation (k_Δ) surrounding the PoP liposomes can be described using eqn (1), where k^{out}, k^{lipid} and k^{in} are the absolute rates of $^1O_2$ deactivation in the bulk solution, the lipid membrane, and the inner liposomal space, respectively. Meanwhile, the values of g are the fractions of the normalized $^1O_2$ lifetime which the species spend in each respective environment, given by eqn (2).

$$k_\Delta = g^{out}k_{out} + g^{lipid}k_{lipid} + g^{in}k_{in} \quad (1)$$

$$g^{out} + g^{lipid} + g^{in} = 1 \quad (2)$$

Commonly, characterization of $^1O_2$ partition between the different phases of a nanocarrier is done through the use of an indirect detection approach, by monitoring the signal of a $^1O_2$ sensitive molecular probe in H_2O and D_2O solvents.[28–30] Due to the heavy isotope effect of the solvent, $^1O_2$ lifetime (τ_Δ) in D_2O is much greater than that in H_2O, therefore quantifying the kinetics of $^1O_2$ production in the two solvents allows for the discrimination of its fraction of lifetime affected (*i.e.* outside of the nanocarrier) and non-affected (*i.e.* inside of the nanocarrier) by the isotope effect.[31] Furthermore, depending on the location of the $^1O_2$ detection probe, researchers have been able to differentiate the amounts of $^1O_2$ present in bulk solution *vs.* the liposomes as a whole; or in the lipid membrane *vs.* the bulk plus the interior liposomal space.[29,30] It is worth noting that to the best of our knowledge no method has been reported to date, which is capable of deciphering all three different contributions to the $^1O_2$ deactivation in a heterogeneous environment in a single, laid out set of experiments.

In our approach, we also take advantage of the method utilizing the heavy isotope effect of the solvent (Scheme 1), and use it in conjunction with quantifying the absolute (*via* direct detection of $^1O_2$ phosphorescence at 1270 nm) and the apparent (*i.e.* how much $^1O_2$ is detected in the bulk solution *via* an indirect method) quantum yields of $^1O_2$ production. The combination of the two methods allows us to discern the difference between the fractions of $^1O_2$ lifetime in all local environments, that is in the outer-, membrane-, and inner-liposomal spaces.

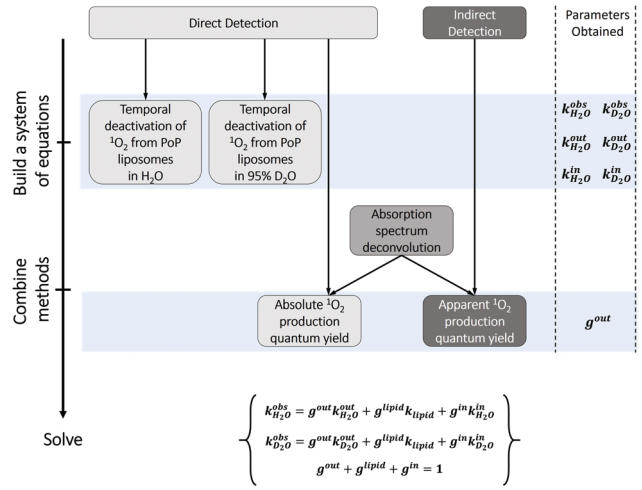

Scheme 1 Outline of the strategy undertaken in this study to quantify the fractions of $^1O_2$ lifetime which the species spend in the external, bulk solution – g^{out}; the liposomal membrane – g^{lipid}; and the internal liposomal cavity – g^{in}.

Experimental

Detailed materials preparation, measurements and data analysis protocols are available in the ESI.† Briefly:

Liposome preparation

PoP liposomes were prepared in a similar way as recently described.[18] PoP liposomes were formed and then actively loaded with either Dox or IRT as described in the ESI,† Section 1.1. Perinaphthenone (PNN, also known as phenalenone)[32] carrying liposomes (PNN@EGG) were used to serve the role of a reference photosensitizer system in the direct detection of $^1O_2$. They were prepared using a standard lipid hydration method (ESI,† Section 1.2).

UV-visible spectra

UV-visible spectra were obtained on dilute liposome solutions (~0.1 mg ml^{-1} in concentration) using a Varian Cary 50 spectrophotometer (ESI,† Section 3.1). Spectral deconvolution was performed *via* a subtractive method using a solution of silica to obtain a pure light scattering spectrum, and the scattering-removed absorption profiles of the EMPTY PoP liposomes as pure porphyrin absorption profiles (ESI,† Section 3.2).

Steady state fluorescence emission spectra

Steady state fluorescence emission spectra were obtained on an Edinburgh FLS900 fluorescence spectrometer with excitation set to 410 nm for general characterization (ESI,† Sections 3.1), or 590 nm for drug release monitoring (ESI,† Section 3.3).

Singlet oxygen phosphorescence detection

Singlet oxygen phosphorescence detection was performed by means of a customized near-infrared (NIR) detection system equipped with a Nd:YAG laser working at a 1 kHz repetition rate at 355 nm or 532 nm, and a Hamamatsu NIR detector (ESI,† Section 4.1).

Broadband irradiation

Broadband irradiation of samples, used in the DOX@PoP drug release studies, and in the indirect detection of $^1O_2$, was performed using a CW halogen lamp (300 W, 80 V) mounted on a slide projector (Kodak), and equipped with an appropriate optical filter (625 nm high-pass for drug release experiments; 295 nm high-pass for indirect detection of $^1O_2$). In the case of the drug-release experiments, samples received ~110 mW of light, or ~8 mW in the case of indirect $^1O_2$ detection (ESI,† Sections 3.3 and 4.2, respectively).

Results and discussion

Material characterization

UV-vis absorption and fluorescence emission. Absorption and emission profiles for the range of PoP liposomes consisted of a sum of several components (Fig. 2 and ESI,† Fig. S2–S6). In the case of EMPTY PoP liposomes (ESI,† Fig. S2 and S8), the total absorption profile consisted of the liposome's light scattering, and of the porphyrin's absorption with the Soret band located at ~419 nm, and the major Q-band at ~674 nm. Obtaining the emission spectrum of the EMPTY PoP revealed that these liposomes carry a single sharp emission band centred at a wavelength of ~675 nm (ESI,† Fig. S2).

Meanwhile the absorption of DOX@PoP (ESI,† Fig. S3 and S9) and IRT@PoP (ESI,† Fig. S5 and S10) liposomes was found to be a sum of three components: liposome's light scattering, as well as the porphyrin and the encapsulated drug absorption. For both drug-carrying systems, the porphyrin's absorption profile was found not to shift significantly compared to the EMPTY PoP (within the monochromator's error of ±1 nm). Similarly, the emission profile of DOX@PoP and IRT@PoP liposomes

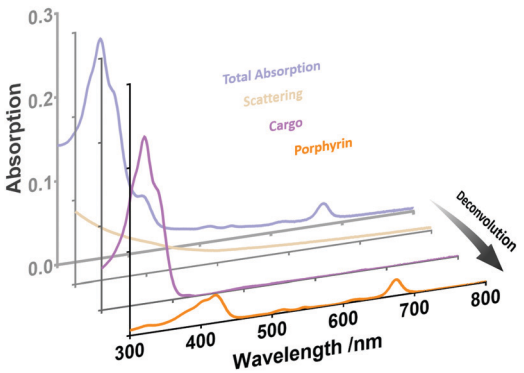

Fig. 2 Sample UV-visible absorption spectral deconvolution for IRT@PoP liposomes. Total absorption of the sample (blue) is matched to a scattering profile obtained on a pure-scattering silica solution (yellow). The difference between the two profiles is referred to as "scattering-removed" absorption (ESI,† Section 3.2) which can be further deconvoluted into the absorption due to the porphyrin (orange), using the scattering-removed absorption of the EMPTY liposomes, and due to the encapsulated drug (purple).

contained identical signatures to that for EMPTY PoP liposomes, in addition to the encapsulated drug emission.

In the case of DOX@PoP liposomes, the absorption profile of the encapsulated DOX was characterized by a broad absorption in the 400–600 nm region, peaking at ~495 nm. Furthermore, it appeared to be overall blue shifted compared to the free drug in solution (ESI,† Fig. S4), suggesting the encapsulated drug aggregation, consistent with previous literature studies.[23] This observation is also concurrent with TEM images of DOX@PoP liposomes which reveal DOX taking on an elongated fibrous shape inside the PoP liposomes (Fig. 1c).[18]

In the case of IRT@PoP liposomes, the encapsulated IRT was found to differ greatly in its absorption profile when compared to its free counterpart in solution (ESI,† Fig. S5 and S6). Overall, the encapsulated IRT was found to have its peak and shoulder absorption change in their relative intensities and undergo a blue shift. Similar to the case of DOX carrying liposomes, we speculate that the changes to the IRT absorption upon encapsulation are induced by the chromophore's confined environment within the internal liposomal cavity.

Importantly for the remainder of this study (*vide infra*), we were able to quantitatively deconvolute each component's contribution to the overall PoP liposomes' absorption (Fig. 2 and ESI,† Fig. S8–S10). As quantifying the quantum yields of $^1O_2$ production under different irradiation conditions was necessary to decipher its partition into the various local liposomal environments, the deconvolution of total PoP liposomes absorption served two important purposes. Firstly, it allowed us to disregard scattering contributions from the quantum yield calculations, assuming that the total light gain in solution due to scattering was negligible.[33] This assumption was justified given the low working concentration of liposomes used throughout the study (<0.1 mg ml^{-1}), thus giving low optical densities of the samples (ESI,† Fig. S2–S7). Secondly, it allowed us to quantify the contribution of the porphyrin *vs.* the encapsulated drug (cargo) absorption to the total absorption of the drug carrying liposomes under various irradiation conditions (*i.e.* the absorption value at 355 nm – A_{355nm}, and the integrated absorption under broadband irradiation conditions – $I_{200–800nm}$; Table 1 and ESI,† Tables S1 and S4). This, in turn, enabled the quantification of individual component contributions to the $^1O_2$ production quantum yields, ultimately painting a clear picture of the synergy between the two chromophores present in these systems.

Solvent stability. As part of our strategy to characterize the partition of $^1O_2$ between the different local environments of the PoP liposomes involved the use of D_2O, we have performed basic liposome characterization experiments to ensure that the liposomes remain structurally indifferent to the deuterated solvent environment.

Dynamic light scattering (DLS) was used to obtain hydrodynamic radii of the PoP liposomes suspended in both H_2O and 95% D_2O solvents (ESI,† Section 2.2). It was found that DOX@PoP, and IRT@PoP had a monodispersed size distribution in water with *z*-average hydrodynamic radius values in the 100–110 nm range (ESI,† Fig. S1). These results were consistent with the TEM images of the samples (Fig. 1b and c). EMPTY PoP liposomes were found to have a broader size distribution, and a higher *z*-average hydrodynamic radius of ~167 nm.

Interestingly, the hydrodynamic radii of all liposomes increased consistently, by ~20 nm, when the samples were suspended in 95% D_2O (ESI,† Fig. S1). Despite this change, each liposome sample appeared to retain its morphology as characterized by the shape and width of the Gaussian *z*-average size distributions in DLS. The observed apparent swelling of the liposomes upon introduction to the deuterated solvent may be an artefact of hydrodynamic radii measurement as the solvation sphere around the liposomes differs between H_2O and D_2O due to the difference in the solvent's hydrogen bonding strength.[34] Moreover, we cannot dismiss the fact that the observed difference may be also due to the liposomes experiencing different degrees of hypotonic stress in either of the solvents, which may lead to swelling.[34–36] Detailed investigations into this phenomenon are beyond the scope of this work; however, it is important for this study to explore the effects of potential hypotonic stress on the stability of drug loaded PoP liposomes.

To ensure that the drug-carrying PoP liposomes do not release their cargo upon a sudden change in the solvent environment caused by D_2O, we performed sample drug release experiments in both H_2O and 95% D_2O solvents (ESI,† Section 3.5, Fig. S13 and S14). Conveniently, drug release from DOX@PoP liposomes can be easily monitored *via* steady-state fluorescence emission measurements.[22,23] Under selective porphyrin irradiation conditions, DOX@PoP liposomes were found to efficiently release DOX when suspended in either the regular or the deuterated water. Notably, liposomes suspended in 95% D_2O were found to release the drug ~7 fold faster than those suspended in H_2O. Importantly, this observation does not necessarily suggest that the PoP liposomes are structurally less stable in D_2O, and is rather consistent with a known phenomenon of deuterated solvent equilibration across the lipid membranes.[35,37,38] Considering that $^1O_2$ has close to an order of magnitude longer lifetime in deuterated water,[39] it is rational that the improved longevity of $^1O_2$ leads to higher probability of activating the drug-release mechanism through the reaction between $^1O_2$ and the unsaturated lipids when the DOX@PoP liposomes are suspended in D_2O.

The above argument was further reinforced by the additional DLS and ζ-potential measurements performed on the DOX@PoP liposomes before and after the drug release (ESI,† Fig. S15). Results of these measurements suggest that the drug release mechanism occurs without the disassembly of the

Table 1 PoP liposome deconvoluted absorption % contributions to the total scattering-removed absorption at select wavelengths

	$A_{355nm}^{porphyrin}$ (%)	A_{355nm}^{cargo} (%)	$I_{200–800nm}^{porphyrin}$ [a] (%)	$I_{200–800nm}^{cargo}$ [a] (%)
EMPTY PoP	100	—	100	—
DOX@PoP	74	26	12	88
IRT@PoP	5	95	73	27

[a] Integral absorption values account for the broadband irradiation source spectrum and the cut-off filter used in the indirect detection of $^1O_2$ (ESI, Section S4.2).

liposomes in both solvents, consistent with previous literature.[40,41] This was concluded based on the shape and width of the *z*-average size distribution plots which were found to be identical before and after the irradiation, concurrent with the surface of the liposomes gaining a more negative charge character after the drug release, which has been shown to be a consequence of unsaturated lipid oxidation caused by $^1O_2$.[27,41]

Based on the results of the above physical characterization experiments, we conclude that the PoP liposomes studied herein remained largely unperturbed in their structure and functionality when suspended in 95% D_2O *vs.* H_2O, thus allowing us to move forward with our strategy to quantify $^1O_2$ partition (Scheme 1).

Singlet oxygen production

Direct detection of singlet oxygen deactivation. The rates of $^1O_2$ deactivation were obtained directly by characterizing each of the three PoP liposome systems *via* the time resolved near-infrared detection set-up, schematically shown in Fig. 3a (details are provided in the ESI,† Section 4.1).[42] Samples dispersed in H_2O or 95% D_2O were excited at 355 nm, corresponding to the excitation of the porphyrin's Soret band. Time-resolved emission was then collected at the signature $^1O_2$ emission wavelength of 1270 nm (Fig. 3c and d and ESI,† Fig. S16–S19). Notably, we have ensured that the collected signal is indeed originating from the $^1O_2$ emission, rather than potential porphyrin phosphorescence, by performing control measurements on N_2 purged samples. In the absence of oxygen, no signal at 1270 nm was detected, indicating that under air-equilibrated conditions the signal at 1270 nm originates from $^1O_2$ only (ESI,† Fig. S18).

Due to the nature of the photosensitization process (ESI,† Scheme S1), the basic kinetic parameters that contribute to the $^1O_2$ production and decay are the lifetime of the photosensitizer's triplet state, τ_T, and the $^1O_2$ lifetime, τ_Δ.[43] Therefore, the phosphorescence signal (S_t) of $^1O_2$ detected at 1270 nm presents a rise and decay bi-exponential behaviour, which can be modelled by the expression given by eqn (3).[42,44] S_0 is the measure of the signal strength, directly linked to the amount of $^1O_2$ present in solution, while the term Y_0 is added to account for the baseline in the real measurement.

$$S_t = S_0 \times \frac{\tau_\Delta}{\tau_\Delta - \tau_T} \times \left(e^{-t/\tau_\Delta} - e^{-t/\tau_T}\right) + Y_0 \qquad (3)$$

It is important to note that in a heterogeneous system, such as liposomes, fitting eqn (3) to the experimentally obtained data gives the average τ_Δ value across the encountered environments (Fig. 3b). While modifications of eqn (3) can be made to account for a heterogeneous environment,[28,45] we were unable to accurately fit such variants to the obtained $^1O_2$ phosphorescence decays in the analysis of different PoP liposome systems.

Average $^1O_2$ lifetimes for the EMPTY PoP and DOX@PoP liposomes were found to be similar in H_2O, with values of 7.1 ± 0.6 μs and 8.0 ± 0.3 μs, respectively (ESI,† Table S2). Furthermore, for IRT@PoP liposomes the observed $^1O_2$ lifetime was found to be strikingly larger in the H_2O environment at 11.1 ± 0.4 μs. It is worth noting that, τ_Δ for a standard photosensitizer free in H_2O is around 3–4 μs (ESI,† Table S5).[31] In comparison, the larger values of τ_Δ obtained for PoP liposome systems are in the range of those previously reported in the literature for liposome suspensions,[46,47] and are themselves indicative of the fact that $^1O_2$ must spend a significant fraction of its overall lifetime in the lipid environment, where typically the deactivation occurs in the tens of microseconds time range.[48,49] Similar trends were found for samples in 95% D_2O with observed τ_Δ values found to be 35.6 ± 0.7 μs, 37.3 ± 0.8 μs and 58.4 ± 0.9 μs for EMPTY PoP, DOX@PoP and IRT@PoP liposomes, respectively (ESI,† Table S2). Meanwhile, for a reference photosensitizer, riboflavin, free in 95% D_2O, the τ_Δ was 37.9 ± 0.2 μs (ESI,† Table S3). The less significant difference between τ_Δ values from the PoP liposomes and the free photosensitizer in 95% D_2O solutions suggests that, in our case specifically, τ_Δ^{lipid} must be similar to $\tau_\Delta^{free\ in\ 95\%\ D_2O}$.

The difference in singlet oxygen lifetime detected from EMPTY PoP *vs.* IRT@PoP can be explained by the fact that in the case of IRT@PoP liposomes, irradiation of samples at a wavelength of 355 nm results primarily in the excitation of the encapsulated IRT (Table 1), which is a known photosensitizer.[50,51] Indeed, performing direct detection of $^1O_2$ phosphorescence on samples of free IRT in H_2O and 95% D_2O confirmed this (ESI,† Fig. S22). Interestingly, for samples of IRT in H_2O, we found τ_Δ to be well above the anticipated 3–4 μs; furthermore the value was also found to increase non-linearly with an increase in IRT concentration until a plateau around 8.7 ± 0.7 μs at >100 μM in IRT concentration (ESI,† Fig. S24). On the other hand, for IRT in 95% D_2O singlet oxygen lifetime did not appear to have a dependence on IRT concentration and was found to average at 40.5 ± 0.3 μs. We speculate that the observed behaviour is due to irinotecan's structure and its ability to locally disturb the

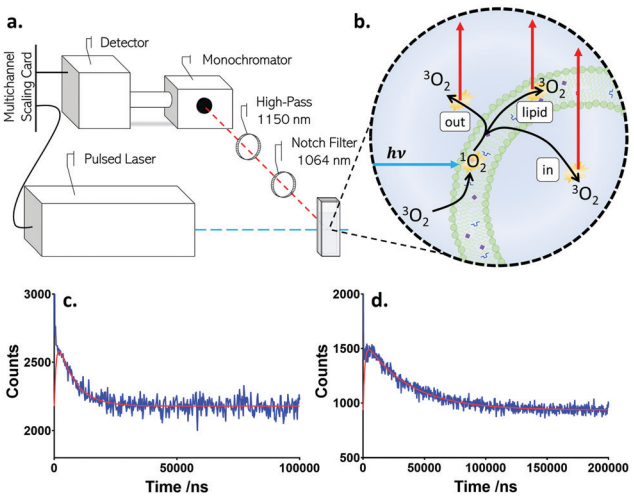

Fig. 3 (a) Schematic of the set-up used for the direct detection of $^1O_2$ emission. (b) Cartoon representation of the $^1O_2$ photosensitization and emission process, notably $^1O_2$ emission originates from all three of the local liposomal environments. (c) In H_2O, and (d) in 95% D_2O – sample $^1O_2$ emission data (blue), and their fit following eqn (3) (red), obtained from EMPTY PoP liposomes (residuals and standard fit errors for all samples and controls are available in the ESI,† Section 4.1).

surrounding hydrogen bonding networks which serve as a dominant pathway for singlet oxygen deactivation in water.[31,52] Given the relative contribution of cargo *vs.* porphyrin to the total absorbance (Table 1), in the case of IRT@PoP liposomes and under our experimental conditions for direct detection, the source of $^1O_2$ is largely IRT itself rather than the membrane bound PoP. Thus, $^1O_2$ is produced largely in the inner liposomal cavity of the liposomes, which undergoes an enhancement in its lifetime due to the solvation environment influenced by the IRT, resulting in the τ_Δ which is significantly larger than that in the EMPTY PoP liposomes.

To understand the similarity in the τ_Δ values obtained for the DOX@PoP and EMPTY PoP liposome samples, we have also characterized the $^1O_2$ behaviour in the presence of free doxorubicin in both solvents. While DOX has been previously reported to have a singlet oxygen production quantum yield of $\sim$0.02,[53] in our experimental set-up (free DOX samples were prepared in similar optical density to DOX@PoP liposomes) DOX by itself was not found to be a $^1O_2$ producer (ESI,† Fig. S23). Furthermore, DOX was also not found to be a $^1O_2$ quencher as it did not influence the τ_Δ when it was added in various concentrations to a solution of standard photosensitizer, riboflavin (ESI,† Fig. S25). Interestingly, addition of DOX to a solution of riboflavin did reduce the photosensitizer's ability to produce $^1O_2$, which suggests that DOX can act as a triplet excited state quencher. This observation is consistent with the fact that DOX has been previously characterized to have its triplet state energy around 151–176 kJ mol^{-1},[53] which is similar to a wide range of common photosensitizers, including some porphyrins.[54] For the purposes of this study, in the case of DOX@PoP liposomes, it is rational to treat the encapsulated DOX as a "silent partner" to the membrane porphyrin. DOX does not produce significant amounts of $^1O_2$ nor quenches it and thus does not alter the observed τ_Δ values of the liposomes. Although, we do not dismiss the possibility of DOX quenching some of the porphysome's ability to produce $^1O_2$ (*vide infra*).

Quantification of the τ_Δ values from a range of PoP liposomes, and free drugs in solution begins to pave a way to obtain $^1O_2$ deactivation rate constants for all three local environments of the liposomes. To achieve this, we first built a system of eqn (4) and (5), based on eqn (1), which we used as a strategy to solve for the fractions of $^1O_2$ lifetime, *i.e.* values of *g*, in each respective environment (Scheme 1).

$$k^{obs}_{H_2O} = g^{out}k^{out}_{H_2O} + g^{lipid}k_{lipid} + g^{in}k^{in}_{H_2O} \quad (4)$$

$$k^{obs}_{D_2O} = g^{out}k^{out}_{D_2O} + g^{lipid}k_{lipid} + g^{in}k^{in}_{D_2O} \quad (5)$$

Under our experimental conditions (low laser power, and slow pulse rate) we anticipate all of the photosensitization process to be monophotonic. Therefore, the observed τ_Δ values are related to the average rates of $^1O_2$ deactivation (k^{obs}) across the three different environments surrounding the liposomes through eqn (6).

$$k_{obs} = 1/\tau_\Delta \quad (6)$$

Using τ_Δ obtained from the PoP liposomes, values of k^{obs} were obtained and are presented in Table 2. Furthermore, the values of τ_Δ from samples of free standard photosensitizers in solution were used to calculate the rates of $^1O_2$ deactivation in the bulk solution (k^{out}). Meanwhile, the lifetimes of $^1O_2$ for samples of a standard photosensitizer, riboflavin, in the presence of DOX, and for the free IRT in solution were assumed to be a sound measure of $^1O_2$ deactivation rate constants in the internal liposomal spaces (k^{in}) of the EMPTY PoP, DOX@PoP and IRT@PoP liposomes, respectively.

Absolute and apparent singlet oxygen production quantum yields. With the obtained rates of $^1O_2$ deactivation, the overall problem can be viewed as a system of three equations (eqn (4), (5) and (2)) and four unknowns (g^{out}, g^{lipid}, g^{in}, and k^{lipid}, Scheme 1). To solve the whole system, we first sought out to independently determine the value of one more variable for each of the PoP liposome systems (Scheme 1). Through careful consideration of $^1O_2$ production kinetics, we realized a way to determine the value of g^{out} though a combination of direct and indirect $^1O_2$ detection methods, namely through the determination of the absolute ($\Phi_\Delta^{absolute}$) and apparent ($\Phi_\Delta^{apparent}$) $^1O_2$ production quantum yields. In the case of direct detection of $^1O_2$ luminescence, the $^1O_2$ signal is detected from all three local liposomal environments, and thus can be used to obtain the $\Phi_\Delta^{absolute}$ values. On the other hand, a $^1O_2$ sensitive molecular probe which only responds to the reactive species present in the bulk solution outside of the nanocarriers can be used to determine the $\Phi_\Delta^{apparent}$ values. The combination of the two methods allowed us to discriminate for the value of g^{out}, as discussed below.

Quantum yields of $^1O_2$ production were obtained from the direct detection of the species luminescence at 1270 nm following eqn (7).[55]

$$\Phi_\Delta^S = \Phi_\Delta^R \times \frac{S_0^S}{S_0^R} \times \frac{\left(1 - 10^{-A^R_{\lambda ex}}\right)}{\left(1 - 10^{-A^S_{\lambda ex}}\right)} \quad (7)$$

As mentioned above, the term S_0 (signal strength in eqn (3)) is directly linked to the amount of luminescent $^1O_2$ present in solution.[45] In the case of PoP liposome systems, $^1O_2$ is produced in the membrane environment, but can further diffuse to either the outer-, or the inner-liposomal space. During this process $^1O_2$

Table 2 Rates of singlet oxygen deactivation obtained *via* the direct detection[a]

	$k^{obs}_{H_2O}/10^4$ s^{-1}	$k^{obs}_{D_2O}/10^4$ s^{-1}	$k^{out}_{H_2O}/10^4$ s^{-1}	$k^{out}_{D_2O}/10^4$ s^{-1}	$k^{in}_{H_2O}/10^4$ s^{-1}	$k^{in}_{D_2O}/10^4$ s^{-1}
EMPTY PoP	14.1 ± 1.1	2.81 ± 0.06	23.8 ± 0.6	2.64 ± 0.01	23.8 ± 0.6	2.64 ± 0.01
DOX@PoP	12.5 ± 0.5	2.68 ± 0.05			23.8 ± 1.7	2.59 ± 0.01
IRT@PoP	9.0 ± 0.3	1.71 ± 0.02			11.5 ± 0.3	2.47 ± 0.02

[a] Errors are based on the standard deviation of fitting eqn (3) to the direct detection data.

encounters local environments with different refractive indexes, polarizabilities, and dielectric properties, all of which have been shown to affect the probability of $^1O_2$ to emit a photon.[56] Thus, the only justifiable way of treating $^1O_2$ luminescence strength as a tool to measure $^1O_2$ production, in eqn (7), is to use a reference photosensitizer system which closely models the same local environment changes as the PoP liposome samples, *i.e.* a standard photosensitizer with a known $^1O_2$ production quantum yield in liposomes. Unfortunately, to the best of our knowledge such a reference system has not been reported to date. In order to alleviate this problem, we chose to work with perinaphthenone (PNN) and synthesize PNN@EGG liposomes to serve as a photosensitizer reference (ESI,† Section 1.2). PNN was chosen as the standard $^1O_2$ producer for several reasons: it can be excited at 355 nm, matching the excitation of PoP liposomes; its $^1O_2$ production quantum yield is nearly constant in a vast range of solvents (Φ_Δ^R = 0.95); and it is lipophilic.[32] Meanwhile, L-α-phosphatidylcholine (egg. chicken) lipids were chosen due to their composition being a mixture of saturated and unsaturated fatty acids, similar to PoP liposomes.

In order to ensure accuracy in the quantum yield values determined using the reference approach, $^1O_2$ direct detection for all liposome systems in H_2O was performed on several unique samples varying in concentration (and thus optical density at 355 nm). Resulting data were analysed using eqn (3) (*vide supra*) and the signal intensities were plotted against the absorption factors, as per eqn (7), using the deconvoluted absorption values at 355 nm (Table 1). Resulting plots (Fig. 4) were fit with a linear equation where the slopes correspond to a $S_0/(1 - 10^{-A_{ex}})$ ratio.

For EMPTY PoP and DOX@PoP liposomes, $^1O_2$ production quantum yields were found to carry an average value of 0.66 and 0.58, respectively (Table 3). Notably, the Φ_Δ value for DOX@PoP liposomes was found to be slightly smaller than that

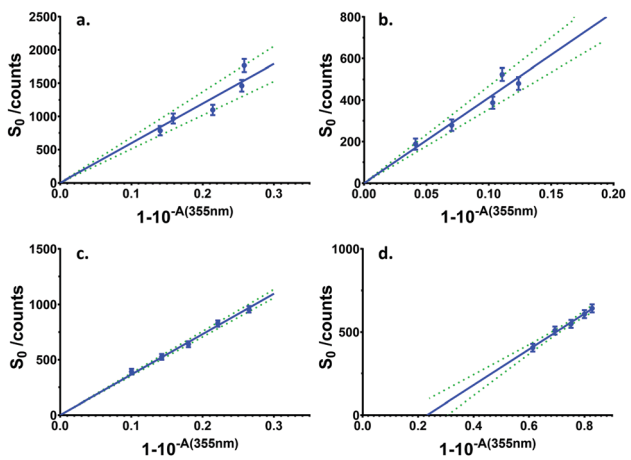

Fig. 4 Evolution of the intensity of the time-resolved $^1O_2$ phosphorescence signals at 1270 nm obtained from the samples of PNN@EGG (a), EMPTY PoP (b), DOX@PoP (c), and IRT@PoP (d) liposomes at different concentrations in H_2O. Error bars represent ± standard deviation obtained from the fits of eqn (3) to the experimental data. Green dotted lines represent the 95% confidence intervals of the best linear fits (blue solid line).

Table 3 Singlet oxygen production quantum yields obtained *via* the direct and the indirect detection

Method/reference system	Direct[a]/PNN@EGG (Φ_Δ = 0.95)	Indirect[b]/RB in the presence of UA (Φ_Δ = 0.66 ± 0.02)
EMPTY PoP[c]	0.66 ± 0.05	0.13 ± 0.01
DOX@PoP[c]	0.58 ± 0.03	0.12 ± 0.01
IRT@PoP[d]	0.17 ± 0.01	0.08 ± 0.01

[a] Errors are based on the standard deviation of fitting eqn (3) to the direct detection data. [b] Errors are based on the standard deviation of fitting eqn (8) to the indirect detection data. [c] Fully deconvoluted values for the porphyrin absorption were used in the calculations. [d] Scattering deconvoluted values for the porphyrin + cargo absorption were used in the calculations.

for the EMPTY PoP, in agreement with the results of $^1O_2$ lifetime characterization in the presence of free DOX which suggested some degree of photosensitizer excited state quenching by the doxorubicin. It is worth noting that in the case of DOX@PoP quantum yield calculations, the absorption of DOX at 355 nm was removed by spectral deconvolution as this species' was not found to be a $^1O_2$ producer (*vide supra*).

On the other hand, the same could not be done for IRT@PoP samples, as IRT itself was found to produce $^1O_2$. As mentioned above, at 355 nm, 95% of the scattering-removed absorption for IRT@PoP samples is due to the IRT itself (Table 1). Having two photosensitizer species present in solution, is likely the reason for the observation in Fig. 4d where the *x*-intercept of the best fit line does not land at the origin point. Furthermore, the value of $^1O_2$ production quantum yield for IRT@PoP was found to be much lower (Φ_Δ = 0.17 ± 0.01) than that for the EMPTY PoP or DOX@PoP liposomes. With the above arguments in mind, we conclude this to be a reasonable outcome since IRT free in solution was characterized to have a $^1O_2$ production quantum yield of 0.11 ± 0.02 (based on the data presented in the ESI,† Section 4.1).

Next, $^1O_2$ production was monitored *via* the indirect detection approach where only $^1O_2$ which makes its way outside of the PoP liposomes can be detected (Fig. 5a and b). In order to ensure the latter, we chose to work with uric acid as a $^1O_2$ detection probe ($\lambda_{abs.max}$ = 291 nm). Uric acid is well known to interact with triplet exited states of some photosensitizers, including porphyrins.[57] Importantly, we did not observe statistically significant changes to the $^1O_2$ production abilities of the PoP liposomes in the presence of uric acid *via* the direct detection (ESI,† Fig. S33 and Table S6), indicating that no direct contact between the photosensitizer and the probe is taking place. This allowed us to conclude that uric acid does not interact with the lipid bound photosensitizer under the timescale of our indirect detection protocol, and thus is only able to detect $^1O_2$ in the bulk external solution phase of the liposomes.

Changes to the uric acid absorption upon the reaction with $^1O_2$ can be described by a pseudo-first order kinetic model, with the integrated rate law given by eqn (8) (derivation in the ESI,† Section 4.2).

$$\ln[UA]_t = \ln[UA]_0 - k_{PS}t \quad (8)$$

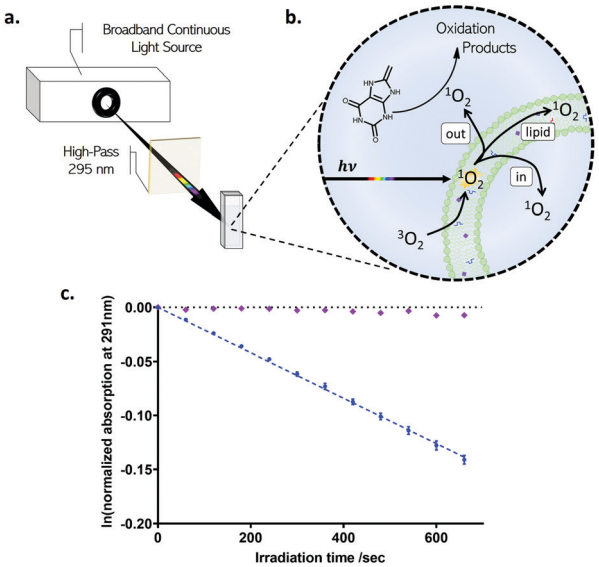

Fig. 5 (a) Schematic of the sample irradiation set-up used in the indirect detection of $^1O_2$. (b) Cartoon representation of the $^1O_2$ photosensitization and reaction with the $^1O_2$ detection probe, uric acid; notably $^1O_2$ can only be detected *via* the reaction with the probe in the external liposomal environment. (c) Sample $^1O_2$ production kinetic data for DOX@PoP liposome samples in H_2O, where the purple diamonds are for N_2 purged samples, and blue circles are for samples exposed to air. Error bars represent ± standard deviation for triplicate measurements. Blue dotted line is the line of best fit of eqn (8) to the experimental data.

The rate constant k_{PS} is simply a combination of a few constants given by eqn (9), where $\Phi_\Delta^{absolute}$ is the absolute quantum yield of $^1O_2$ production, I_{Abs} being the integrated intensity of the absorbed light (ESI,† Table S1), and k_{ox} the rate constant of uric acid oxidation.

$$k_{PS} = -g^{out} \times k_{ox} \times \Phi_\Delta^{absolute} \times I_{Abs} \times \frac{1}{k} \quad (9)$$

By monitoring the uric acid absorption signal disappearance upon selective sample irradiation, values of k_{PS} were determined experimentally for the PoP liposomes and the reference PS system (sample data in Fig. 5c; all data in the ESI,† Fig. S27–S31). The apparent $^1O_2$ production quantum yields for PoP liposome systems were then determined using a reference approach, and following eqn (10) (Table 3, derivation in the ESI,† Section 4.3). In this case, Rose Bengal was used as a reference sensitizer, and its known interaction with uric acid[57] has been accounted for (ESI,† Section 4.4).

$$\Phi_\Delta^{apparent} = \Phi_\Delta^R \times \frac{k_{PS}^S}{k_{PS}^R} \times \frac{I_{Abs}^R}{I_{Abs}^S} \times \frac{\tau_\Delta^R}{\tau_\Delta^S} \quad (10)$$

Final results of the indirect detection measurements are presented in Table 3 (details are provided in the ESI,† Sections 4.3 and 4.4). It was found that for all PoP liposome systems studied, only a small fraction of the total produced $^1O_2$ can be detected in the bulk solution.

Partition of singlet oxygen into the local liposomal environments. Notably, $^1O_2$ produced from the reference photosensitizer in a homogeneous environment, as in the case of indirect detection, spends all its lifetime in the solvent; thus by definition, the value of g^{out} for the reference is equal to 1 (eqn (9)). Consequently, based on eqn (9) and (10), the apparent $^1O_2$ production quantum yields for the liposome systems obtained using this approach are defined by eqn (11) (derivation in the ESI,† Section 4.3).

$$\Phi_\Delta^{apparent} = g^{out} \times \Phi_\Delta^{absolute} \quad (11)$$

Care was taken when considering the meaning behind the values of $\Phi_\Delta^{absolute}$ in the context of indirect *vs.* direct detection of $^1O_2$. This is because direct detection was performed at a single excitation wavelength of 355 nm, while indirect detection was performed using a broad range of the visible spectrum (ESI,† Fig. S26). For the EMPTY PoP and the DOX@PoP liposomes, the porphyrin present in the liposomal membrane is the sole contributor to the $^1O_2$ production. Thus, it was safe to extrapolate that, as both the direct and the indirect $^1O_2$ photosensitization experiments involved the irradiation of the same single $^1O_2$ producer, the values of Φ_Δ obtained *via* direct detection can be used directly as $\Phi_\Delta^{absolute}$ in equation 11 to obtain the values of g^{out} for each system (Table 4). On the other hand, the same cannot be said for IRT@PoP liposome samples, as both the IRT and the membrane porphyrin are $^1O_2$ producers (*vide supra*). As mentioned previously, based on spectral deconvolution, at 355 nm, 95% of all absorption for IRT@PoP samples is due to the IRT (Table 1), whereas, under the broadband irradiation conditions only 24% of total absorption is due to the encapsulated drug. Given that these absorption contribution values are known, the Φ_Δ values of the EMPTY PoP liposomes and of the free IRT obtained *via* the direct detection can be used to estimate $\Phi_\Delta^{absolute}$ for IRT@PoP under the broadband irradiation conditions to be 0.53 ± 0.04 (ESI,† Section 4.5). This value was used in eqn (11) to calculate the fraction of $^1O_2$ which escapes into the bulk solution.

The obtained g^{out} values for all PoP liposome systems are presented in Table 4, and all fall in a similar range of ~0.15–0.20, which is in line with the previously mentioned trends between the direct and indirect detection approaches. Overall this result indicates that whether the liposomes do or do not carry cargo does not significantly affect their ability to release $^1O_2$ into the bulk solution.

With the values of g^{out} quantified, the system of eqn (4), (5) and (2) can be solved for the three remaining unknowns: k^{lipid}, g^{lipid} and g^{out} (Scheme 1, ESI,† Section 4.6). The value of k^{lipid} was determined to be 30 ± 3 × 10^4 s^{-1} for the EMPTY PoP

Table 4 Fractions of $^1O_2$ lifetime spent in the different local environments of PoP liposomes[a]

	g^{out}	g^{lipid}	g^{in}
EMPTY PoP	0.19 ± 0.02	0.47 ± 0.04	0.34 ± 0.06
DOX@PoP	0.20 ± 0.02	0.54 ± 0.07	0.26 ± 0.09
IRT@PoP	0.14 ± 0.02	0.50 ± 0.08	0.36 ± 0.10

[a] ±standard deviation values are reported based on the propagation of error resulting from the direct and indirect $^1O_2$ detection measurements.

liposomes and is in the range of typically reported values for $^1O_2$ deactivation in lipids and surfactants (ESI,† Section 4.6).[39,48,49] Since the lipid composition was the same for all PoP systems, this value was further used in g^{lipid} quantification for all three PoP liposome formulations together with the data from the direct detection in either H_2O or 95% D_2O solvents (Table 2, ESI,† Section 4.6). Lastly, the values of g^{out} were obtained using eqn (2) using the remaining quantified values of g presented in Table 4.

Despite some differences in their photophysical behavior, all three versions of the PoP liposomes were found to carry out $^1O_2$ release in a similar manner. Through the novel approach of combining direct and indirect $^1O_2$ detection measurements, we found that >80% of all sensitized $^1O_2$ from the PoP liposomes deactivates within the nanostructures themselves. In the case of EMPTY PoP liposomes, which were found to produce $^1O_2$ with a staggering 0.66 quantum yield, only ~19% of all $^1O_2$ was found to deactivate in the bulk solution, with the majority of $^1O_2$ remaining in the lipid membrane (~47%) and some (~34%) deactivating in the inner-liposomal cavity. Although DOX@PoP liposomes were found to have a slightly lower absolute quantum yield of $^1O_2$ production (0.58) this material behaved similarly to the EMPTY PoP liposomes in terms of its $^1O_2$ releasing abilities. For DOX@PoP liposomes, $^1O_2$ was found to spend ~20% of its lifetime in the bulk external solution environment, with the remaining ~54% and ~26% spent in the lipid membrane and the internal liposomal cavity, respectively. Lastly, due to the presence of two photosensitizing species, IRT@PoP liposomes were found to have a variable $^1O_2$ production quantum yield depending on the wavelength of excitation. Under our experimental conditions, in the case of monochromatic excitation at 355 nm, IRT@PoP absorption was dominated 19 : 1 by the encapsulated IRT which resulted in a $^1O_2$ production quantum yield of only 0.17, similar to the value for free IRT in solution (0.11). While $^1O_2$ partition from the IRT@PoP liposomes under broadband irradiation conditions was ultimately characterized to consist of ~14% contribution in the outer-, ~50% contribution in the membrane-, and ~36% contribution in the inner-liposomal environments, we speculate these numbers to also be dependent on the irradiation wavelength(s) as $^1O_2$ is able to be produced from both the liposomal cavity and the lipid membrane locations. Notably even with only ~26% and ~36% of the produced $^1O_2$ reaching the internal liposomal cavity, for DOX@PoP and IRT@PoP liposomes respectively, some degree of the encapsulated drug's degradation was noted *via* UV-visible spectroscopy after prolonged 355 nm laser irradiation (ESI,† Fig. S35).

Conclusions

Through several basic spectroscopic techniques, we were able to deduce that in the case of EMPTY PoP and DOX@PoP liposomes the photophysical properties of the materials are dictated largely by the membrane-trapped porphyrin chromophore. On the other hand, in IRT@PoP liposomes the encapsulated IRT was also confirmed to be a $^1O_2$ producer, which altered this material's photosensitizing behavior under different irradiation conditions.

All formulations of PoP liposomes were found to be well behaved in terms of their $^1O_2$ releasing abilities. EMPTY PoP and DOX@PoP liposomes behaved nearly identically, despite the DOX@PoP liposomes carrying chemotherapeutic cargo. DOX was found to be largely a non-interfering, silent partner to the membrane porphyrin. Both of these liposome formulations were characterized to have an absolute $^1O_2$ production quantum yield in the ~0.6–0.7 range, and have the ability to release ~1/5 of all produced $^1O_2$ into the bulk solution while keeping ~1/2 of all $^1O_2$ in the lipid membrane. On the other hand, IRT@PoP liposomes were found to have a more complex photophysics most evident in the $^1O_2$ production quantum yield measurements, which were found to be dependent on the excitation conditions due to both the membrane porphyrin and the encapsulated IRT acting as photosensitizers. Nevertheless, similar to the other two PoP liposome formulations tested, IRT@PoP was also found to confine ~1/2 of all produced $^1O_2$ in the lipid membrane, while releasing ~1/6 of sensitized $^1O_2$ into the bulk solution. The fast drug-release kinetics of the PoP systems can now be understood from the relative $^1O_2$ partition values reported herein. Based on the majority of the produced $^1O_2$ deactivating in the lipid membrane of the PoPs, we have confirmed this material to be well suited for dual-action chemo/phototherapy.

We believe our study to be a useful tool for researchers in the field of nano-biomaterial design seeking to use our approach to quantify their material's abilities to release $^1O_2$ into the specific local liposomal space. As we have discovered in the case of PoP liposomes, that a large fraction of $^1O_2$ staying in the membrane liposomal environment may be advantageous for fast-acting chemotherapeutic drug release. However, modifications to the lipid composition, or the size of the vesicles, may be made to tailor the material properties to be more photo-therapeutic, with more $^1O_2$ being released into the bulk solution, and slower chemotherapeutic drug release, as may be desired.

Conflicts of interest

J. F. Lovell is a co-founder of POP Biotechnologies. Other authors declare no conflicts.

Acknowledgements

The authors would like to thank Dr David J. Press and Nicolas Macia for their contribution to the advancement of the project. We would also like to extend our gratitude to the Natural Sciences and Engineering Research Council of Canada (NSERC), the University of Calgary and CFI for financial support. V. K. gratefully acknowledges NSERC for an Alexander Graham Bell Canada Graduate Doctoral Scholarship.

Notes and references

1 D. E. J. G. J. Dolmans, D. Fukumura and R. K. Jain, *Nat. Rev. Cancer*, 2003, **3**, 380–387.
2 M. R. Detty, S. L. Gibson and S. J. Wagner, *J. Med. Chem.*, 2004, **47**, 3897–3915.
3 I. J. Macdonald and T. J. Dougherty, *J. Porphyrins phthalocyanines*, 2001, **5**, 105–129.
4 R. W. Redmond and I. E. Kochevar, *Photochem. Photobiol.*, 2006, **82**, 1178–1186.
5 P. Sharma, M. Mehta, D. S. Dhanjal, S. Kaur, G. Gupta, H. Singh, L. Thangavelu, S. Rajeshkumar, M. Tambuwala, H. A. Bakshi, D. K. Chellappan, K. Dua and S. Satija, *Chem.-Biol. Interact.*, 2019, **309**, 108720.
6 M. Olek, J. Kasperski, D. Skaba, R. Wiench, G. Cieślar and A. Kawczyk-Krupka, *Photodiagn. Photodyn. Ther.*, 2019, **27**, 255–267.
7 S. S. Lucky, K. C. Soo and Y. Zhang, *Chem. Rev.*, 2015, **115**, 1990–2042.
8 N. L. Oleinick and H. H. Evans, *Radiat. Res.*, 1998, **150**, S146–S156.
9 H.-B. Cheng, Y. Cui, R. Wang, N. Kwon and J. Yoon, *Coord. Chem. Rev.*, 2019, **392**, 237–254.
10 G. Obaid, M. Broekgaarden, A. L. Bulin, H. C. Huang, J. Kuriakose, J. Liu and T. Hasan, *Nanoscale*, 2016, **8**, 12471–12503.
11 Y. Shen, A. J. Shuhendler, D. Ye, J.-J. Xu and H.-Y. Chen, *Chem. Soc. Rev.*, 2016, **45**, 6725–6741.
12 N. M. Idris, M. K. G. Jayakumar, A. Bansal and Y. Zhang, *Chem. Soc. Rev.*, 2015, **44**, 1449–1478.
13 Y.-Y. Wang, Y.-C. Liu, H. Sun and D.-S. Guo, *Coord. Chem. Rev.*, 2019, **395**, 46–62.
14 Y. Lee and D. H. Thompson, *Stimuli-responsive liposomes for drug delivery*, 2017.
15 D. Luo, J. Geng, N. Li, K. A. Carter, S. Shao, G. E. Atilla-Gokcumen and J. F. Lovell, *Mol. Cancer Ther.*, 2017, **16**, 2452.
16 M. Karimi, P. Sahandi Zangabad, S. Baghaee-Ravari, M. Ghazadeh, H. Mirshekari and M. R. Hamblin, *J. Am. Chem. Soc.*, 2017, **139**, 4584–4610.
17 D. Luo, K. A. Carter, A. Razi, J. Geng, S. Shao, C. Lin, J. Ortega and J. F. Lovell, *J. Controlled Release*, 2015, **220**, 484–494.
18 K. A. Carter, D. Luo, A. Razi, J. Geng, S. Shao, J. Ortega and J. F. Lovell, *Theranostics*, 2016, **6**, 2329–2336.
19 S. Ghosh, R. Qi, K. A. Carter, G. Zhang, B. A. Pfeifer and J. F. Lovell, *Biochem. Eng. J.*, 2019, **141**, 43–48.
20 K. A. Carter, S. Wang, J. Geng, D. Luo, S. Shao and J. F. Lovell, *Mol. Pharmaceutics*, 2016, **13**, 420–427.
21 K. A. Carter, S. Shao, M. I. Hoopes, D. Luo, B. Ahsan, V. M. Grigoryants, W. Song, H. Huang, G. Zhang, R. K. Pandey, J. Geng, B. A. Pfeifer, C. P. Scholes, J. Ortega, M. Karttunen and J. F. Lovell, *Nat. Commun.*, 2014, **5**, 3546.
22 D. Luo, N. Li, K. A. Carter, C. Lin, J. Geng, S. Shao, W.-C. Huang, Y. Qin, G. E. Atilla-Gokcumen and J. F. Lovell, *Small*, 2016, **12**, 3039–3047.
23 K. Nawara, P. Krysinski and G. J. Blanchard, *J. Phys. Chem. A*, 2012, **116**, 4330–4337.
24 D. Miranda, N. Li, C. Li, F. Stefanovic, G. E. Atilla-Gokcumen and J. F. Lovell, *ACS Appl. Nano Mater.*, 2018, **1**, 2739–2747.
25 H. Mojzisova, S. Bonneau, P. Maillard, K. Berg and D. Brault, *Photochem. Photobiol. Sci.*, 2009, **8**, 778–787.
26 A. Barras, N. Skandrani, M. Gonzalez Pisfil, S. Paryzhak, T. Dumych, A. Haustrate, L. Héliot, T. Gharbi, H. Boulahdour, V. Y. Lehen'kyi, R. Bilyy, S. Szunerits, G. Bidaux and R. Boukherroub, *J. Mater. Chem. B*, 2018, **6**, 5949–5963.
27 I. O. L. Bacellar, M. C. Oliveira, L. S. Dantas, E. B. Costa, H. C. Junqueira, W. K. Martins, A. M. Durantini, G. Cosa, P. Di Mascio, M. Wainwright, R. Miotto, R. M. Cordeiro, S. Miyamoto and M. S. Baptista, *J. Am. Chem. Soc.*, 2018, **140**, 9606–9615.
28 V. Kabanov, D. J. Press, R. P. S. Huynh, G. K. H. Shimizu and B. Heyne, *Chem. Commun.*, 2018, **54**, 6320–6323.
29 M. Hoebeke and X. Damoiseau, *Photochem. Photobiol. Sci.*, 2002, **1**, 283–287.
30 M. Hoebeke, J. Piette and A. van de Vorst, *J. Photochem. Photobiol., B*, 1991, **9**, 281–294.
31 J. R. Hurst and G. B. Schuster, *J. Am. Chem. Soc.*, 1983, **105**, 5756–5760.
32 R. Schmidt, C. Tanielian, R. Dunsbach and C. Wolff, *J. Photochem. Photobiol., A*, 1994, **79**, 11–17.
33 N. Macia, V. Kabanov, M. Côté-Cyr and B. Heyne, *J. Phys. Chem. Lett.*, 2019, **10**, 3654–3660.
34 C. H. Chen, *J. Phys. Chem.*, 1982, **86**, 3559–3562.
35 N. Tokutake, B. Jing and S. L. Regen, *Langmuir*, 2004, **20**, 8958–8960.
36 R. Bittman and L. Blau, *Biochemistry*, 1972, **11**, 4831–4839.
37 E. A. Disalvo, O. A. Pinto, M. F. Martini, A. M. Bouchet, A. Hollmann and M. A. Frías, *Biochim. Biophys. Acta, Biomembr.*, 2015, **1848**, 1552–1562.
38 R. M. Venable, A. Krämer and R. W. Pastor, *Molecular Dynamics Simulations of Membrane Permeability*, 2019.
39 F. Wilkinson, W. P. Helman and A. B. Ross, *J. Phys. Chem. Ref. Data*, 1995, **24**, 663–677.
40 O. Mertins, I. O. L. Bacellar, F. Thalmann, C. M. Marques, M. S. Baptista and R. Itri, *Biophys. J.*, 2014, **106**, 162–171.
41 S. Sankhagowit, S.-H. Wu, R. Biswas, C. T. Riche, M. L. Povinelli and N. Malmstadt, *Biochim. Biophys. Acta, Biomembr.*, 2014, **1838**, 2615–2624.
42 S. Nonell and S. E. Braslavsky, *Methods in Enzymology*, Academic Press, 2000, vol. 319, pp. 37–49.
43 R. Schmidt and H. D. Brauer, *J. Am. Chem. Soc.*, 1987, **109**, 6976–6981.
44 A. Krasnovsky Jr, *Mol. Membr. Biol.*, 1998, **12**, 665–690.
45 G. Zampini, O. Planas, F. Marmottini, O. Gulias, M. Agut, S. Nonell and L. Latterini, *RSC Adv.*, 2017, **7**, 14422–14429.
46 J. Baier, M. Maier, R. Engl, M. Landthaler and W. Bäumler, *J. Phys. Chem. B*, 2005, **109**, 3041–3046.
47 A. Molnár, R. Dědic, A. Svoboda and J. Hála, *J. Mol. Struct.*, 2007, **834–836**, 488–491.
48 S. J. Dearden, *J. Chem. Soc., Faraday Trans. 1*, 1986, **82**, 1627–1635.
49 M. A. J. Rodgers, *Photochem. Photobiol.*, 1983, **37**, 99–103.

50 V. Brezova, M. Valko, M. Breza, H. Morris, J. Telser, D. Dvoranova, K. Kaiserova, L. Varecka, M. Mazur and D. Leibfritz, *J. Phys. Chem. B*, 2003, **107**, 2415–2425.
51 M. Bobeničová, M. Valko, V. Brezová and D. Dvoranová, *J. Photochem. Photobiol., A*, 2014, **290**, 125–138.
52 M. Bregnhøj, M. Westberg, F. Jensen and P. R. Ogilby, *Phys. Chem. Chem. Phys.*, 2016, **18**, 22946–22961.
53 A. Andreoni, E. J. Land, V. Malatesta, A. J. McLean and T. G. Truscott, *Biochim. Biophys. Acta, Gen. Subj.*, 1989, **990**, 190–197.
54 A. C. M. Montalti, L. Prodi and T. M. Gandolfi, *Handbook of Photochemistry*, CRC Press, 3rd edn, 2006.
55 G. Boso, D. Ke, B. Korzh, J. Bouilloux, N. Lange and H. Zbinden, *Biomed. Opt. Express*, 2016, **7**, 211–224.
56 B. M. Dzhagarov, E. S. Jarnikova, M. V. Parkhats and A. S. Stasheuski, *Opt. Spectrosc.*, 2014, **116**, 926–932.
57 M. Bregnhøj, L. Dichmann, C. K. McLoughlin, M. Westberg and P. R. Ogilby, *Photochem. Photobiol.*, 2019, **95**, 202–210.

